GMR
The Original

DEVELOPMENT OF NOVEL ANTIBACTERIAL BIOACTIVE COATINGS ON MAGNESIUM BASED IMPLANTS TO TREAT INTRA-ARTICULAR FRACTURES

Hira Fatima[1], Sohail Nadeem[1*], Farasat Iqbal[2]

[1] Department of Chemistry, University of Management and Technology, Lahore, 54770 Pakistan.
[2] Interdisciplinary Research Centre in Biomedical Materials, COMSATS University Islamabad, Lahore Campus, Pakistan.
*Corresponding Author: Dr. Sohail Nadeem, Email: sohail.nadeem@umt.edu.pk

ABSTRACT
Magnesium (Mg) and its alloys have emerged as viable biodegradable materials for orthopedic implants because of their advantageous mechanical compatibility and bioresorbability properties; nevertheless, their rapid corrosion, hydrogen evolution, and infection susceptibility limit their clinical application. In the current study, phosphate coatings were fabricated on pure Mg and AZ31 Mg alloy through a single-step hydrothermal synthesis approach with Ag and Cu being added to improve the antibacterial and corrosion resistance properties. Reaction temperature and an alkaline pH environment were optimized from 125 to 200 °C and 9.0, respectively, for coating nucleation and growth. Structural features were examined by scanning electron microscope (SEM) and X-ray diffraction (XRD) analysis. The electrochemical behavior was evaluated through potentiodynamic polarization and open circuit potential measurements. In vitro degradation was assessed in simulated body fluid (SBF) at 37 °C, and antibacterial performance was determined against *Staphylococcus aureus* and *Escherichia coli* using the broth dilution method. From the results obtained, hydrothermal treatment was shown to facilitate the in-situ synthesis of dense magnesium phosphate layers through the dissolution–re-precipitation process, with significant temperature-induced morphology modifications. A highly dense structure free from defects with 98% reduction in the corrosion rate as compared to bare Mg was observed at 150 °C. AZ31 samples containing 0.05 M% Ag showed the most balanced overall performance. These findings highlight a viable strategy to regulate Mg degradation while imparting antibacterial functionality for biodegradable implant applications.

KEYWORDS: Biomaterials, Anti-bacterial Bioactive Coating, Magnesium based implants, Intra-Articular Fractures, Biodegradation rate

1. INTRODUCTION

The prevalence of bone fractures and other related abnormalities due to factors such as age, trauma, sports injuries, and other degenerative conditions has contributed to the high demand for advanced biomaterials for bone repair and reconstruction (Paiva *et al.* 2022). Modern-day orthopedic implants serve an essential role in the treatment of inter- and intra-articular fractures that are characterized by either a break in the continuity of the bone at the joint region or dislocations, making treatment very difficult (Gueorguiev *et al.* 2017, Misir 2025). Intra-articular fractures have become even more challenging since these are located in highly active joints. Conventional methods of treatment that utilize plates and rods have proven inadequate in such cases (Farjam *et al.* 2022). Thus, various types of fixation systems using screws, pins, rods, and wires have been designed and used to treat fractures (Stiffler 2004, Schatzker 2005). While these implants have produced excellent results (Nuss *et al.* 2008), their permanence makes secondary surgery inevitable to remove these devices once the fracture is healed (Vos *et al.* 2013, Muralidharan *et al.* 2023). This procedure poses many challenges for patients since the implant is difficult to remove completely and may end up damaging the surrounding (Schlickewei *et al.* 2019).

The primary problem with metallic implants is the difference in elasticity between the implant and the natural bone, which interferes with the natural process of stress distribution and creates a condition known as stress shielding (Gefen 2002, Jin *et al.* 2025). Stress shielding results in decreased stimulation of the bone tissues and eventually bone resorption and implant loosening. These issues have prompted researchers to develop biodegradable and biocompatible materials, which mimic the bone structure and degrade in vivo, thus avoiding the necessity for a second surgery (Tabrizian *et al.* 2024). The material should possess low density, adequate mechanical resistance, the ability to integrate with bones, and a controllable degradation rate without toxic waste generation (Sun *et al.* 2025). Magnesium (Mg) and its alloys have been found to possess unique mechanical as well as biological properties (Sharma *et al.* 2022). Mg is one of the lightest metals with a density (≈1.74 g/cm³) similar to natural bones and an elastic

modulus (≈40–45 GPa) considerably low compared to other common materials for implants, hence avoiding stress shielding and providing proper load transfer (Staiger *et al.* 2006, Al-Tamimi *et al.* 2017, Radha *et al.* 2017, Niyou 2021). Furthermore, due to their high specific strength, Mg alloys are considered ideal materials to be used as a load-bearing system (Prakasam *et al.* 2017, Matli *et al.* 2020). In terms of biology, Mg has many functions to perform in the body, including metabolic activities, osteoblast proliferation, and mineral deposition in bones (Lian *et al.* 1992, Yadav *et al.* 2024).

Despite these benefits, the fast corrosion rate of magnesium in physiological surroundings poses a serious problem. When magnesium is in water it reacts with the water to form a layer of magnesium hydroxide on its surface. This layer is not very stable because of the chloride ions that are found in the fluids in our body. These chloride ions break down the magnesium hydroxide layer. Turn it into magnesium chloride that can dissolve in water. This process keeps happening over again which means the magnesium just keeps on corroding (Staiger *et al.* 2006, Brar *et al.* 2009). Hydrogen gas is also released as a product of the corrosion process. The accumulated hydrogen gas results in gas pockets, interfering with adjacent tissues and affecting cell adhesion (Noviana *et al.* 2016). Moreover, the rise in pH levels owing to alkali formation hinders cellular functions and biological processes, eventually resulting in an inability to maintain stability and proper tissue healing (Song 2007, Liu *et al.* 2016, Xu *et al.* 2022). All these factors together impose restrictions on the safe use of Mg-based implants, especially in load-bearing scenarios. There have been several attempts to address these issues through alloying and surface modifications. Despite the advantages associated with alloying magnesium with materials like aluminum, zinc, manganese, and rare earths for enhanced strength and corrosion resistance, doubts persist about their toxic effects and biocompatibility (Song *et al.* 2007, Prawin Babu *et al.* 2025). The same is true for other elements that can be added to increase degradation rate, which might pose certain dangers to health and therefore reduce its usefulness in medical treatments. Therefore, coating materials by bioactive surfaces is seen as a better way to deal with such issues (Hornberger *et al.* 2012, Rahim *et al.* 2017).

Of many coating systems available, calcium and magnesium phosphates coatings have a unique advantage owing to their chemical composition similar to that of natural bone tissue and good bioactivity. In addition to providing protection from corrosion, they also stimulate osteogenesis (Gray-Munro *et al.* 2009, Uppal *et al.* 2021, D'Amado *et al.* 2024). The formation of an apatite layer on the implant surface enhances cell adhesion, proliferation, and differentiation, thereby improving osteointegration (Shadanbaz *et al.* 2012, Bai *et al.* 2018). An apatite coating on the surface of an implant promotes the adhesion, growth, and differentiation of cells, thus improving the process of bone integration. Moreover, higher levels of roughness and surface energy of such coatings promote protein absorption and interaction, which improve the biological and mechanical properties of implants. (Biggs *et al.* 2010). Furthermore, such coatings can substantially lower corrosion rates and hydrogen evolution from metal implants.

In light of the above discussions, this study aims at developing phosphate coatings on pure magnesium and AZ31 Mg alloys by a single step process in which various processing conditions, namely, temperature, pressure, and pH will be optimized to investigate their effects on the morphology, adhesion, and thickness of the coatings. Specific attention is paid to the deposition of both magnesium oxide and phosphate phases as a means of controlling the rate of degradation and hydrogen formation. In addition to structural evaluations, electrochemical and biological assessments of the coatings will be made in order to establish the feasibility of the coating processes in terms of improving the corrosion resistance and cytocompatibility of the coated magnesium materials.

2. MATERIALS AND CHEMICALS

High-purity magnesium (99.98%) and AZ31 magnesium alloy were used as substrate materials, with the composition of AZ31 consisted of Magnesium 90%, Aluminum 3% and Zinc 1%. Both materials were obtained from Goodfellow Cambridge Limited, UK. All chemicals were analytical grade (>99.9% purity) and supplied by Sigma–Aldrich. Di-ammonium hydrogen phosphate ($(NH_4)_2HPO_4$) served as the coating precursor, while ammonium hydroxide (NH_4OH) and nitric acid (HNO_3) were used to adjust the solution pH. Analytical-grade reagents were also used to prepare simulated body fluid (SBF) for in vitro degradation studies.

2.1 Sample Preparation

The pure magnesium was then cut to rectangular shaped samples (10×2 mm), degreased according to ASTM D1732, and washed with distilled water. Then, the samples were polished with different grades of silicon carbide papers (800–1200 grit) to achieve an even surface. Finally, they were cleaned using ethanol and acetone for 5–10 minutes, rinsed, dried under air, and placed in a stainless-steel jar with the reaction mixture.

2.2 Preparation of Phosphate Coating Solution

The phosphate precursor solution was prepared by mixing 0.6M $(NH_4)_2HPO_4$ solution in deionized water. Precisely, the pH value of the solution was set to 9 through drop-wise addition of NH_4OH. In order to completely dissolve all chemicals in the mixture and establish homogeneous chemistry of the solution, magnetic stirring was done at a temperature-controlled hot plate for 30 minutes.

2.3 Preparation of Doped-Phosphate Coating Solution

The phosphate solution was doped using silver nitrate and copper nitrate through a one-step hydrothermal process. A 0.06 M di-ammonium hydrogen phosphate solution was first prepared in deionized water. Next, I added silver nitrate or copper nitrate to the solution. The concentrations of nitrate or copper nitrate added were 0.01 M, 0.05 M and 0.1 M. The solution was then mixed using a stirrer on a hotplate for 30 minutes. This ensured that the dopant ions, silver and copper were well mixed. After that ammonium hydroxide was added dropwise to the solution. The goal was to maintain a pH of 9 in the solution, with silver and copper dopants. The phosphate precursor solution was doped with nitrate and copper nitrate. The doping process used a hydrothermal method. The solution had di-ammonium hydrogen phosphate, silver nitrate and copper nitrate via the hydrothermal method.

2.4 Coating Deposition Using Hydrothermal Method

The hydrothermal deposition of the coating was conducted by a controlled method using a system provided with a Parr 4848 reactor controller. The obtained precursor solution and magnesium alloy samples were introduced into the reaction vessel for forming a closed system. The reactor was heated up to certain temperatures (125, 150, 175, and 200 °C) for 3 h, where both temperature and pressure were monitored in real time by means of a thermocouple and pressure gauge to ensure stable autogenous conditions. In these high thermodynamic conditions, partial dissolution of the magnesium substrate results in the liberation of Mg^{2+} ions that react with phosphate ions to undergo nucleation and growth of magnesium phosphates directly onto the surface of the substrate. In addition, the presence of an alkaline medium (pH 9) contributes to the effective kinetics of precipitation reactions leading to the formation of dense and adherent coatings. The reactor was cooled down to room temperature in an uncontrolled manner in order to stabilize the formed phases. The coated samples were withdrawn from the reactor, washed with deionized water to remove any excess material, and dried in air.

2.4 Preparation of Simulated Body Fluid (SBF)

The simulated body fluid (SBF) was made in accordance with the procedure provided by Kokubo et al. The preparation involved mixing all the chemicals in double deionized water as per the values indicated in Table 2.2 to mimic the ionic content of human blood plasma. TRIS was used as the buffer, and the solution was then adjusted to a pH of 7.4 physiologically using 1M hydrochloric acid (HCL). The SBF was left to stabilize for 24 hours before usage. (Kokubo *et al.* 2007).

Table 2.1 Order and amounts of chemical reagents used for the preparation of 1000 ml SBF

Order	Reagents	Amount
1	NaCl	8.035 g
2	$NaHCO_3$	0.355 g
3	KCl	0.225 g
4	$K_2HPO_4{\cdot}3H_2O$	0.231 g
5	$MgCl_2{\cdot}6H_2O$	0.311 g
6	1.0 M-HCL	39 ml + 0-5 ml
7	$CaCl_2$	0.292 g
8	Na_2SO_4	0.072 g
9	Tris	6.118 g

3. RESULTS AND DISCUSSIONS

3.1 Morphological Analysis and Coating Evolution

The morphological features of the surface and cross-section of hydrothermal magnesium phosphate films were greatly affected by the deposition temperature and pH value of the starting material solution, as seen in Figure 3.1. Films formed at 125 °C showed full surface coverage by well-ordered, petallike crystal structures without any defect, suggesting controlled crystallization process under milder conditions. The variant P7125 had the most pronounced floral pattern growing from one nucleus, whereas lowering the pH to 4 changed this morphology drastically; since there was higher Mg^{2+} supersaturation under acidic conditions, the phosphate precipitated rapidly, forming overlapping plate like structures. The pH 9, on the other hand, favored the formation of smaller flower-like structures consisting of flakes standing perpendicular to the substrate.

Coatings subjected to 150 °C had a distinct change in terms of the growth pattern of crystals. Coating of sample P7150 had a shift in growth pattern from the presence of horizontal plates to vertically-aligned flowers, hence improved kinetics of crystal growth. Acidic solution gave rise to surfaces characterized by the existence of layers of stacked horizontal plates. The morphology of the P9150 coating was highly uniform, dense, crack-free, and consisted of a combination of both plate-like and petal-like structures. Cross-sectional observation also showed that the thickness of the coating was decreasing with the increase in pH value, having a thickness of 28.765 µm, 19.765 µm, and 10.284 µm for P4150, P7150, and P9150, respectively. Although thicker coatings could be obtained under acidic condition, coatings produced using alkaline solution were denser. This was due to the controlled release of Mg^{2+} ions and formation of an oxide interface.

In case of heating to high temperature (175 °C), there was degradation of the coating microstructure even though there was an improvement in thickness. The typical flower-like microstructures were altered, forming thick, flake-like microstructures along with micro cracking. The thickness of the coatings was relatively high (184.034 µm, 177.951 µm, and 154.394 µm, for P4175, P7175, and P9175 coatings, respectively); however, the formation of internal stresses associated with fast crystal growth led to the development of interface cracks, resulting in a weak structure that allowed delamination. In case of heating up to 200 °C, there was full phase transformation with compact microstructures with nanocrystalline nature owing to lattice distortion and crystal plane reorientation.

On the whole, results obtained through morphological and thickness measurements show that P9150 coating has the most desirable properties, including well-packed structure without any defects with strong interfacial strength. The described morphology is directly associated with better resistance against corrosion and well-regulated hydrogen production in physiologically relevant environment. Additionally, it was shown that doping could be performed with low silver content (0.01 mol %), which did not disrupt the intrinsic flower-like morphology, but introduced metal particles uniformly distributed between the layers of phosphate. The metal particles increased density of the coating material and helped with stress relaxation, allowing for stable and homogeneous coating morphology formation. Nevertheless, higher amount of silver in coating (0.1 mol %) caused considerable change in its morphology, and the surface of the sample was mostly covered by flake-like structure instead of flowers. The high contrast seen in SEM images can be related to electron backscatter due to high Z atomic number of silver particles.

Likewise, copper doping preserved the morphology at low doses, but the introduction of tetrahedral phases and enhanced porosity occurred at higher doses. The AZ31 alloy samples that had silver added to them looked really consistent with a flower like shape. This was also helped by the metal that was put on them. It was good for making the surface look nice and even. It stopped problems from happening. The AZ31 alloy samples with silver in them were really good for this. In the end we learned that how we made the AZ31 alloy samples and how silver we added to them was very important, for getting magnesium phosphate coatings that work really well for medical use (Ali *et al.* 2019).

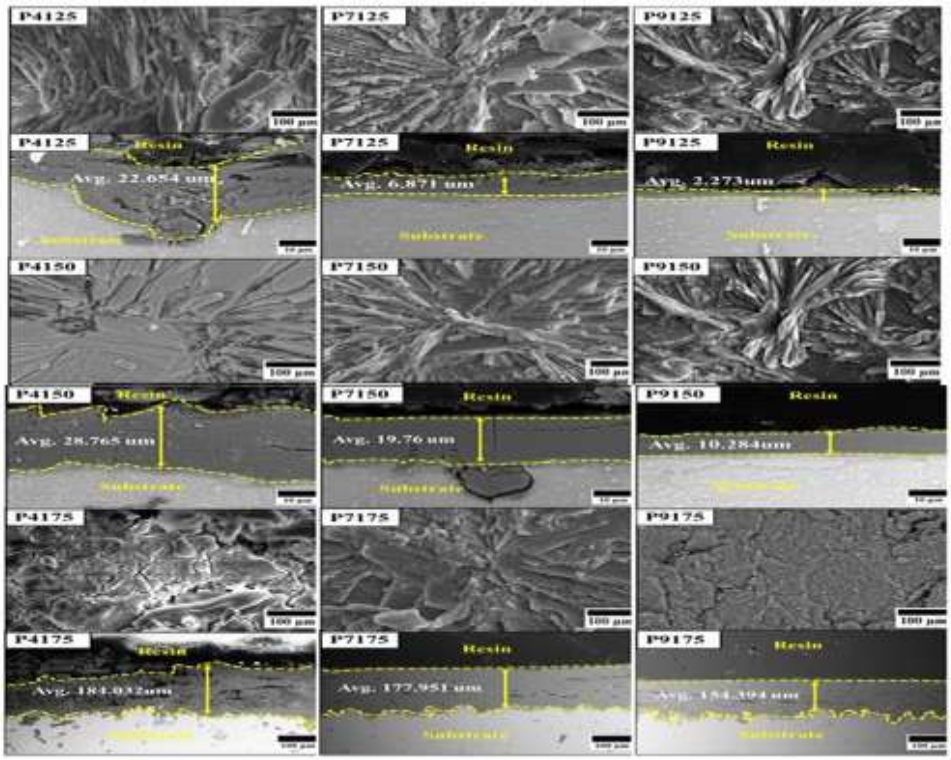

Figure 3.1. SEM images of magnesium phosphate coating surfaces and cross-sections varying with temperature and pH levels

3.2 Structural and Phase Analysis of coated and uncoated samples

The XRD results that are shown in Figure 3.2 show that magnesium phosphate-based films were formed on magnesium. These films have magnesium and other things like brucite and magnesium phosphate in them. They also have magnesium phosphate compounds. The things that are in these films depend on how acidic the solution's that they are made in and how hot it is. If the solution is very acidic like when the pH is 4 then the films will have hydrated phosphate compounds in them. This is because the magnesium dissolves faster in solutions and this makes the crystals form faster. When the pH is higher there are hydrated phosphate compounds and more magnesium phosphate and oxide compounds. The XRD results also show that when the temperature is 150 °C the crystalline peaks are stronger and sharper, than when the temperature's lower. This means that magnesium phosphate-based films are better made at temperatures. The XRD results in Figure 3.2 are important because they help us understand how magnesium phosphate-based films are formed on magnesium.

The phase transformation process is controlled by the primary formation of $Mg(OH)_2$ interphase layer, serving as a hindrance and facilitating localized alkalinity conditions, leading to the interaction of phosphates with Mg^{2+} ions to create a secondary layer of phosphates. An increase in temperature results in the facilitation of ion migration and diffusion, hence speeding up the coating process and phase transformation. Nevertheless, an increase in temperature (175 °C) causes internal stress and lattice distortion, resulting in the degradation of structural integrity, as seen in the formation of micro-cracks during morphological studies

The XRD spectra of doped coatings (Figure 3.2) confirm the incorporation of Ag and Cu within the phosphate matrix. In Ag-doped coatings, the appearance of Ag_3PO_4 and metallic Ag peaks verifies successful deposition, while a reduction in brucite peak intensity and slight peak broadening indicate increased coating thickness and modified crystallinity. Similarly, Cu-doped coatings exhibit copper phosphate phases, with higher concentrations leading to the formation of additional phases such as $Cu_2P_4O_{12}$, suggesting a more complex coating structure. For AZ31 magnesium alloy, similar phase compositions are observed, with moderate Ag content enhancing coating formation, while excessive doping slightly reduces crystallinity due to increased metallic deposition (Hiromoto *et al.* 2009).

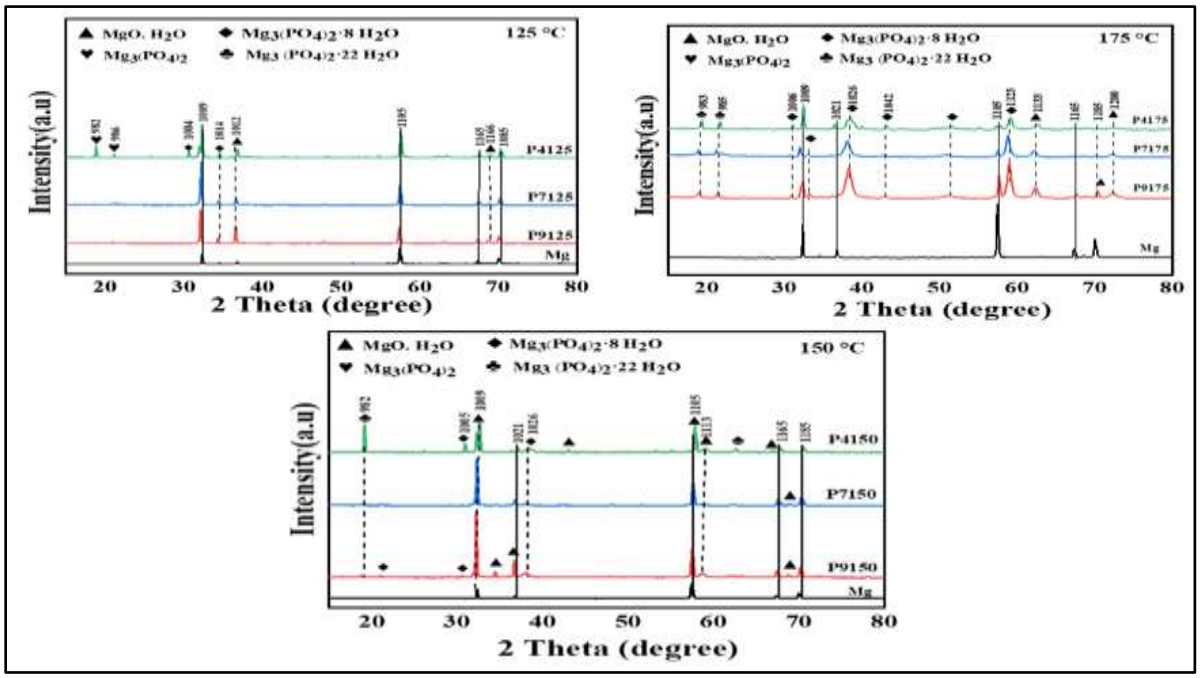

Figure 3.2. XRD spectra of hydrothermally deposited magnesium phosphate on pure magnesium substrate at pH 4, 7, and 9 at temperatures (A) 125°C, (B) 150°C, and (C) 175°C for 3 h.

3.3 Functional Group Analysis

FTIR spectroscopy technique was used in order to identify the bonding properties and functional groups of the deposited coatings through hydrothermal synthesis. The FTIR spectra (see Figures 3.3 & 3.4) show distinct bands in the 400–1400 cm^{-1} region due to P–O, P–O(H), O–P–O(H), and O–P–O bonds that confirm the formation of a magnesium phosphate structure on the substrates' surfaces (Song 2005). The absorption band at approximately 960 cm^{-1} represents the asymmetric stretching vibration of P–O–P bonds, signifying that the pyrophosphate bonding exists in the polymer matrix. Other absorption bands detected at 1065 cm^{-1} represent P–O stretching vibration, while those between 845–725 cm^{-1} indicate C–H vibrations. The weaker absorption band at 1485 cm^{-1} also confirms the presence of organics or carbonates.

Another broad absorption range is observed from 2500 to 3700 cm^{-1}, which can be attributed to the –OH groups, which exist due to the presence of water of hydration and hydrated phosphates. Thus, the existence of structural water in the magnesium phosphate hydrates is indicated by this observation as a result of the hydrothermal synthesis method used. Overall, the FTIR spectrum results are in excellent correlation with XRD results regarding the synthesis of magnesium phosphate (Cacciotti *et al.* 2009, Bakin *et al.* 2016).

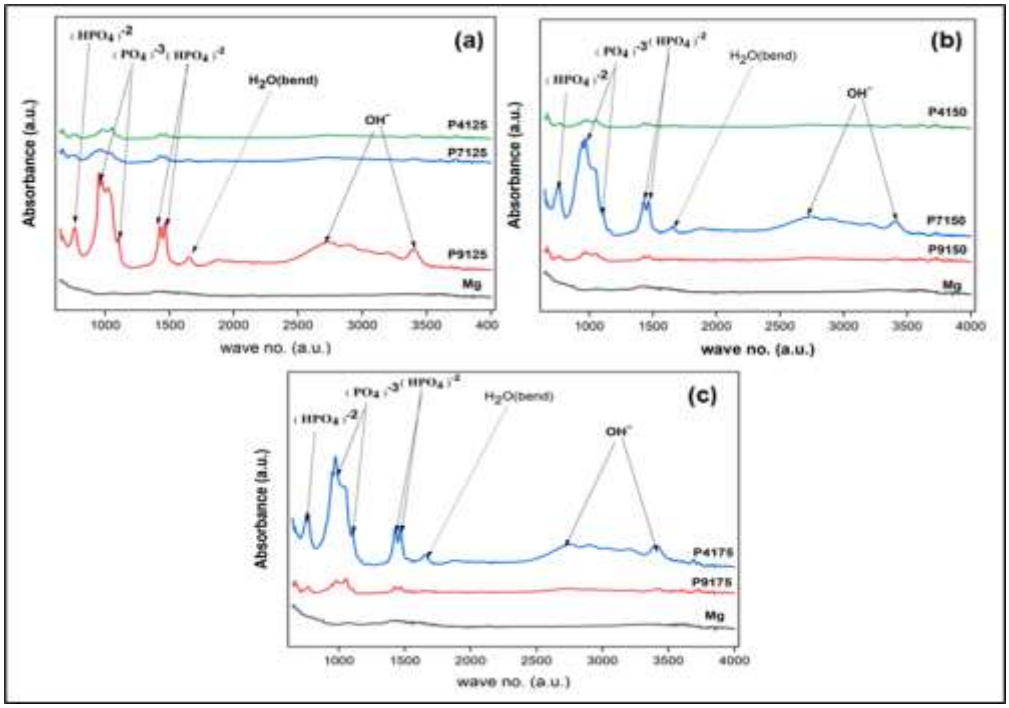

Figure 3.3. FTIR spectra of phosphate coated pure Mg (a) At 125°C on pH 4,7 and 9 (b) At 150 °C on pH 4,7 and 9 (c) At 175°C on pH 4,7 and 9

Moreover, FTIR analysis on Ag and Cu doped films (Figures 4.9a,b) shows functional group similarities with the undoped films, showing that doping with ions does not have any significant impact on the underlying phosphate structure. But differences in peak intensity show changes in crystalline structure and phase content with increasing concentration of dopants. For example, in Ag doped AZ31 films (Figure 4.9c), a higher phosphate peak intensity was found for undoped films and lower concentration of Ag (0.01 and 0.05 mol %), while a decrease in intensity at 0.1 mol % Ag showed the lower formation of phosphate phase due to the excessive incorporation of metal ions.

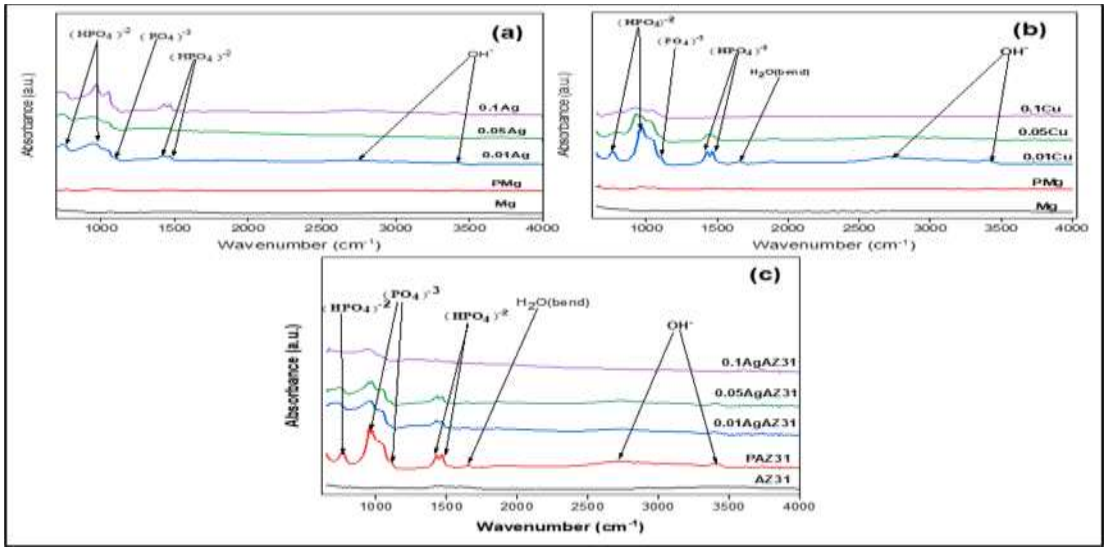

Figure 3.4 FTIR spectra of (a) Silver doped phosphate coated pure Mg at 150 °C on pH 9 (b) Copper doped phosphate coated pure Mg at 150 °C on pH 9 (c) Hydrothermally deposited silver doped phosphate coating on AZ31-Mg alloy at pH 9 on temperatures 150 °C for 3hrs

3.4 Coating Adhesion Strength

The adhesion strength of magnesium phosphate coatings formed via hydrothermal method is one of the main parameters which affect the stability of the coating and its corrosion properties. According to the values obtained from Figure 3.5 and shown below, all the coatings considered here (namely, P4125, P7125, P4150, P7150, P9150, and P7175) have shear strength greater than the value equal to 15 MPa which is required according to ISO 13779-4 standard.

Adhesion performance is mainly determined by microstructural characteristics such as coating density, porosity, crystal size, and microcrack generation. Coatings that are dense and crack-free have high adhesion owing to better load transfer and lesser stress concentration at the interface compared to porous and cracked coatings. This is mainly associated with thermal stresses arising from differences in the coefficient of thermal expansion (CTE) between coating and substrate materials. Low thermal stress is favorable for interface stability, whereas higher stress leads to cracks and weaker adhesion.

Processing variables affect adhesion properties considerably. At 125 °C, the highest adhesion was observed for P7125 because of its dense microstructure. On the other hand, acidic and alkaline solutions caused low adhesion due to increased porosity and microcracking. High temperatures usually led to poor adhesion due to the creation of internal stress and cracking. The exception was pH 9 solution when higher temperatures led to denser and crack-free coatings, leading to better adhesion performance. Temperature 175 °C had the lowest adhesion because of high levels of cracking, especially in P9175. P9150 recorded the highest adhesion strength among the three solutions due to its compact and defect-free structure (Tang *et al.* 2013).

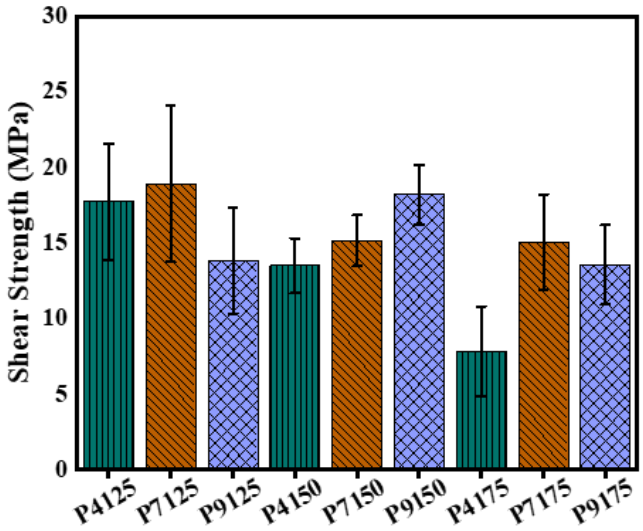

Figure 3.5. Shear strength of magnesium phosphate coatings deposited hydrothermally on pure magnesium substrate at pH levels 4, 7, and 9, at temperatures of 125, 150, and 175ºC

3.5 Corrosion Behaviour of Bare and Coated Mg-Alloy

The corrosion behaviour of bare and coated magnesium samples was investigated in simulated body fluid (SBF) at 37 °C using open-circuit potential (OCP) and potentiodynamic polarization (PDP) techniques. OCP measurements provided information on interfacial stability and passivation behavior, while PDP analysis was used to quantify corrosion parameters such as corrosion potential (E_corr), corrosion current density (I_corr), and corrosion rate via Tafel extrapolation (Table 3.1).

Table 3.1 PDP parameters of bare, Phosphate coated as well as doped with Ag and Cu derived by Tafel extrapolation

Sample ID	$E_{corr.}$ (V)	$I_{corr.}$ (µA/ cm^2)	CR (mpy)
Ag-0.01M	-0.8286	1.983e^{-8}	1.866
Ag-0.05M	-1.231	1.823e^{-8}	42.9
Ag-0.1M	-1.311	4.767e^{-5}	127
Cu-0.01M	-0.4084	4.631e-9	10.92
Cu-0.05M	-0.465	1.234e-8	25.42

Cu-0.1M	-1.595	1.337e-6	387.93
MgP	-1.283	$2.202e^{-7}$	106.1
Pure Mg	-1.417	$4.984e^{-7}$	312.2

The PDP results show that bare magnesium exhibits the highest corrosion activity, with an I_corr of 4.984×10^{-7} A/cm². The application of magnesium phosphate coating significantly reduces corrosion (to 2.202×10^{-7} A/cm²), confirming the formation of a protective barrier layer. Further improvement is observed with low-level Ag and Cu doping, particularly at 0.01 M, where I_corr values decrease substantially, indicating enhanced corrosion resistance. However, at higher dopant concentrations (0.1 M), corrosion resistance deteriorates, suggesting that excessive doping leads to coating defects or reduced compactness, which compromises protection. A similar trend is observed for AZ31 substrates, where coated and lightly Ag-doped samples show markedly improved performance compared to uncoated alloy (Sui *et al.* 2004, Balamurugan *et al.* 2007).

A positive shift in E_corr for coated samples compared to bare magnesium confirms improved passivation and reduced electrochemical activity. This is attributed to the formation of a dense phosphate-based barrier that limits electrolyte penetration and suppresses both anodic dissolution and hydrogen evolution reactions. The increased polarization resistance (R_p) of coated samples further supports their enhanced durability in SBF. Overall, magnesium phosphate coatings, particularly those doped with low concentrations of Ag and Cu, provide effective corrosion protection and controlled degradation behavior, making them suitable for biodegradable implant applications

3.6 Effect of degradation rate on coatings

The degradation performance of uncoated and coated magnesium alloys was analyzed using the body fluid simulator after 14 days of immersion through weight loss determination and hydrogen evolution measurements (Figures 3.6 and 3.7). It can be seen from the findings that there is an evident decrease in the degradation rate of coated magnesium alloys as opposed to uncoated magnesium alloys, indicating that magnesium phosphate coatings offer excellent protection against corrosion processes. The greatest weight loss was observed on the part of the substrate since uncoated magnesium samples showed the highest degradation rate due to the absence of a protective coating. Initially, weight loss was minimal during the first day of immersion; afterwards, it steadily increased.

Degradation properties were greatly affected by processing parameters. For instance, while immersed at 125 °C, certain coated materials (e.g., P4125 and P7125) had greater weight loss compared to bare magnesium in early stages because of their porous nature and defects. While immersed at 150 °C, degradation rates were greatly reduced, with P9150 having the least amount of weight loss among all coatings. The reason behind this superior performance is that it had dense, crack-free structure, which prevented electrolyte from penetrating into magnesium substrates and hence slowed down their degradation rate. However, when immersed at 175 °C, increased porosity and micro-cracking caused higher degradation rates even though lower mass loss was observed initially. Macroscopic observations also confirmed that bare magnesium experienced high corrosion levels and production of white corrosion products.

In addition, dopant concentration was also an important parameter contributing to corrosion properties. The least amount of weight loss was observed for 0.05 M% Ag-doped samples. Higher dopant concentration (Ag - 0.1 M%, Cu - 0.1 M%) caused more severe degradation effects; for example, the latter sample decomposed completely in less than one day. These effects were explained by higher porosity of the coatings, as well as galvanic corrosion of metallic ions with the magnesium matrix and increased solubility of corrosion products ($Mg(OH)_2$). All of the observations described above clearly prove that the best corrosion resistance was achieved by low-to-moderate dopant concentration. Thus, the results of weight loss tests, as well as hydrogen evolution test, proved that among all analyzed variants P9150 had the best resistance to physiological medium (Witte *et al.* 2005, Liu *et al.* 2016).

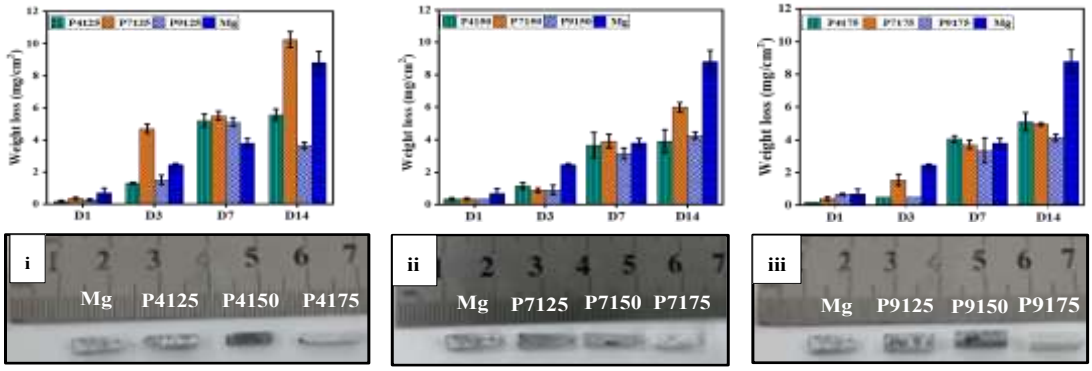

Figure 3.6 (a) Weight loss of hydrothermally deposited coatings after 14-day immersion in SBF at 37°C pH and temperature variants. (b) Macrographs of uncoated and coated samples after immersion time of 14 days in SBF.

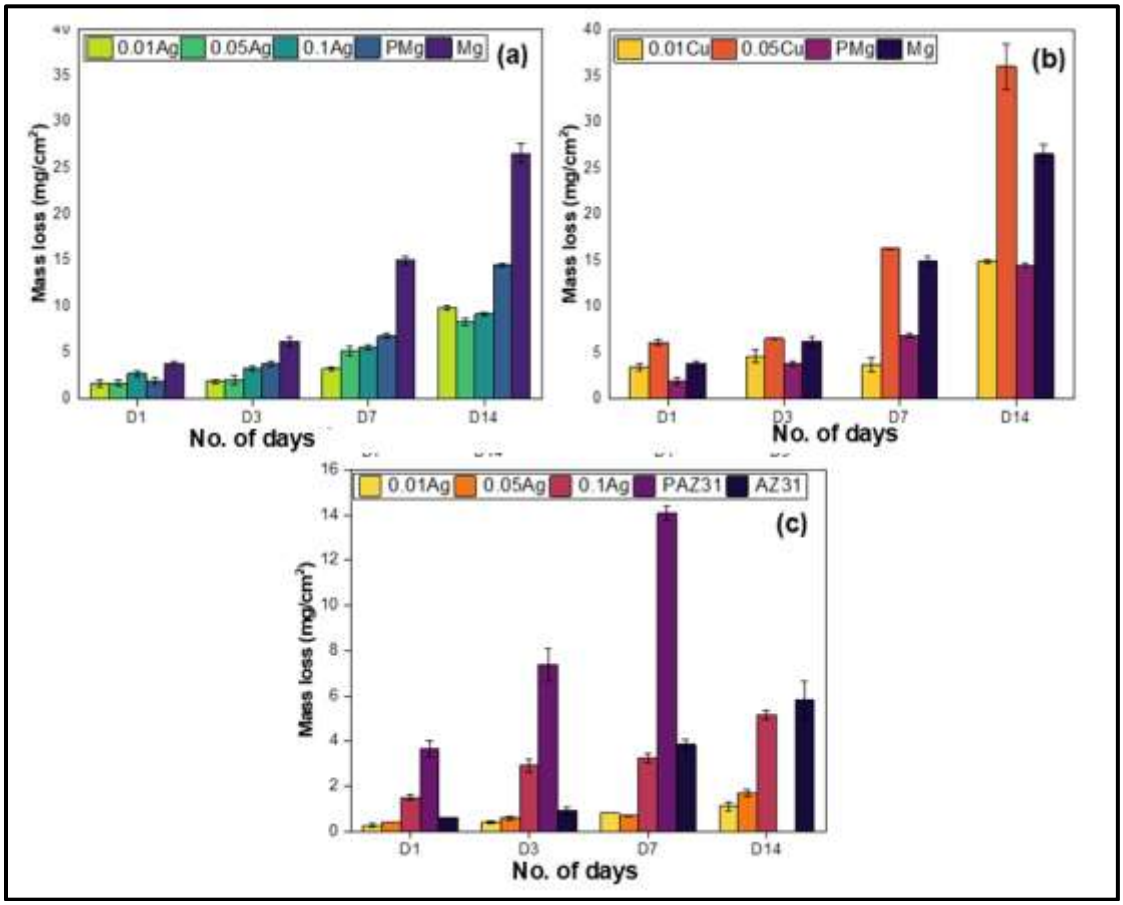

Figure 3.7 Mass loss of hydrothermally deposited (a) Silver doped phosphate coatings after 14-day immersion in SBF at 37°C (b) Copper doped phosphate coatings after 14-day immersion in SBF at 37°C (c) Silver doped phosphate coatings on AZ31-Mg alloy after 14-day immersion in SBF at 37°C

3.7 Effect of coating on behavior of Hydrogen Evolution

The hydrogen evolution rate (HER) for uncoated and coated magnesium samples after immersion in simulated body fluid (SBF) for 14 days at 37 °C is displayed in Figures 3.8 and 3.9. Hydrogen production was maximum and continuously increasing in bare magnesium samples, which shows that corrosion takes place at a faster pace. On the contrary, hydrogen evolution rate for phosphate-coated samples was much lower, indicating successful control of electrolyte–metal contact. It should be noted here that hydrogen evolution is a direct result of magnesium dissolution and the formation of $Mg(OH)_2$, which then dissolves in the presence of Cl^- ions in the form of $MgCl_2$ in SBF, resulting in pitting.

It can be seen from HER results that the effect of processing conditions was quite pronounced in terms of HER as a function of time. Coatings fabricated at 125 °C at pH 4 and 7 had higher HER compared to those produced at other pH values; however, HER decreased after the seventh day due to corrosion product formation, serving as a barrier. Meanwhile, pH 9 coating showed a relatively stable low HER level. When comparing coatings processed at different temperatures, those processed at 150 °C, especially P9150 sample, proved to have the least HER value, and such property is associated with its high-quality structure. At 175 °C, HER increased for all pHs because of the porous structure of coatings.

Doping introduced additional effects on hydrogen evolution properties. Silver-doped coatings demonstrated a dose-dependent effect on HER activity; however, all the readings were below those of pure Mg. The smallest hydrogen evolution was detected for 0.01 M Ag; a slight decrease in the protective effect of coatings with an increase in silver dosage is associated with a higher structure heterogeneity. Copper doping resulted in an abrupt increase in hydrogen evolution, and the sample doped with 0.1 M Cu experienced extremely fast degradation owing to intense galvanic activity of Cu-containing phases and Mg substrate. Thus, HER dynamics correlated very well with weight loss dynamics, which means that structural parameters are responsible for hydrogen evolution and corrosion protection (Radha *et al.* 2017, Chandra *et al.* 2020).

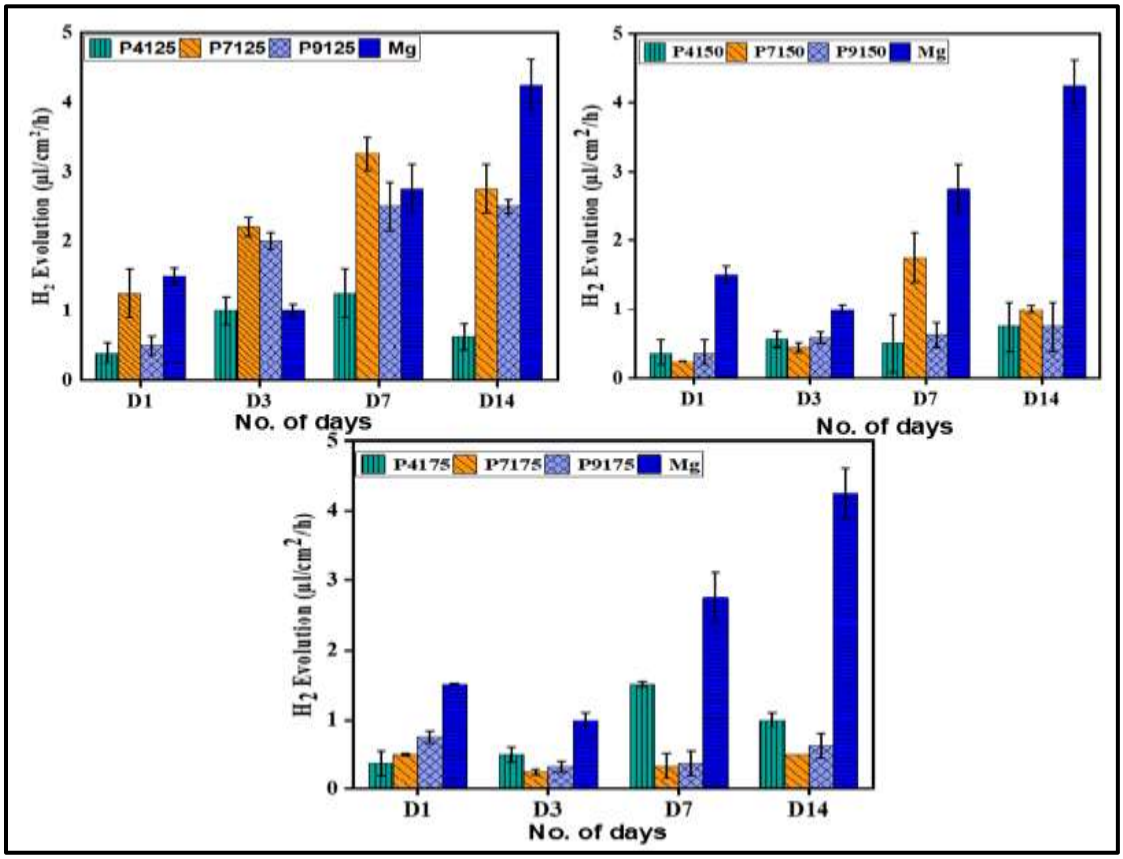

Figure 3.8 H_2 evolution of hydrothermally deposited coating after 14 days immersion in SBF at 37°C pH and temperature variants

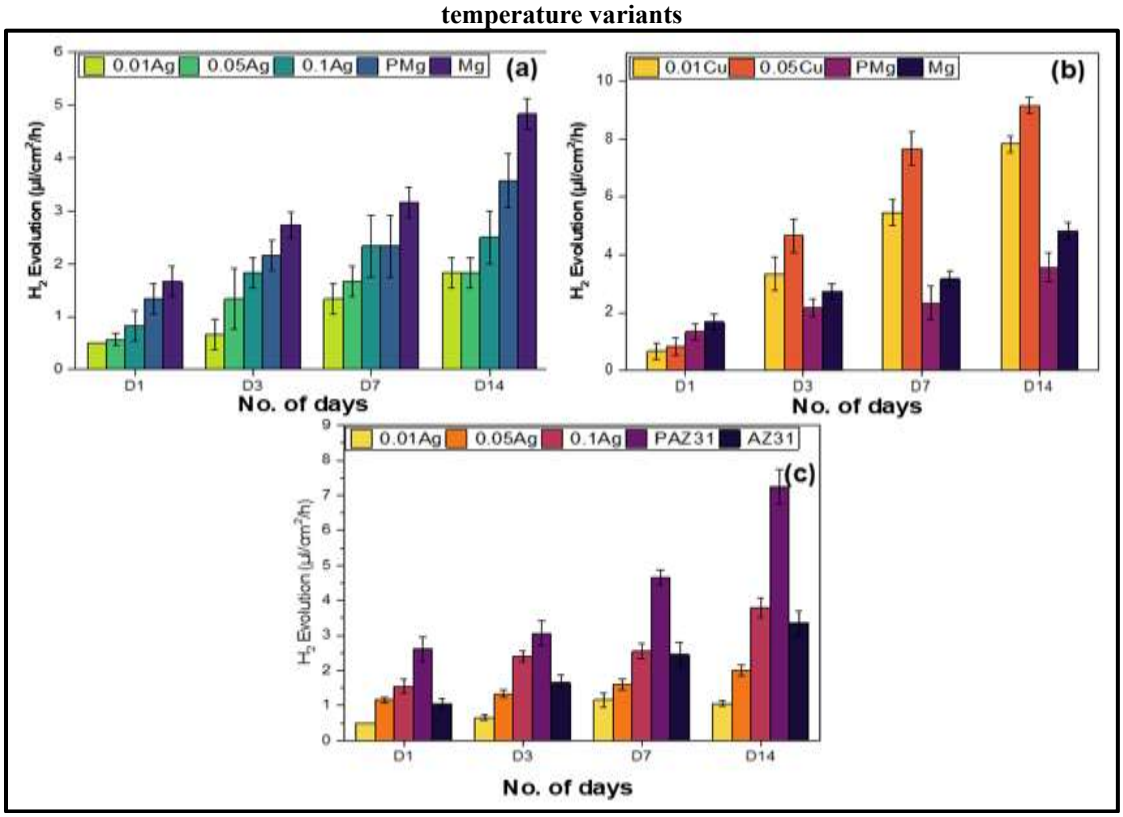

Figure 3.9 H_2 evolution of hydrothermally deposited (a) Silver doped phosphate coatings after 14 day immersion in SBF at 37°C (b) Copper doped phosphate coatings after 14 day immersion in SBF at 37°C (c) Silver doped phosphate coatings on AZ31-Mg alloy after 14 day immersion in SBF at 37°C

3.8 Cytocompatibility Assessment (Alamar Blue Assay)

Cytocompatibility of the Mg substrates coated with phosphates was assessed with the use of pre-osteoblast MC3T3-E1 cells utilizing the Alamar Blue assay at the first, third, and seventh day after the cells seeding. Cell response to biomaterials is very important when estimating the osteoconductive properties of materials, which are formed through a series of events that include cell proliferation, extracellular matrix production, and mineralization. In this experiment, non-coated magnesium was used as the control sample whereas cells without a substrate served as the positive control. In general, all coated and uncoated magnesium surfaces allowed for continued cell proliferation with time, but the phosphate coatings were able to enhance this process through inhibiting rapid magnesium degradation and subsequent alkaline environment around the substrate surface. Overall, the P9150 variant of the phosphate coating demonstrated the highest cell viability values on both day 3 and day 7, which is a result of optimal surface morphology characterized by high homogeneity and lack of defects. Meanwhile, magnesium specimens with faster degradation kinetics demonstrated reduced metabolic activity in later experimental stages as a result of faster magnesium ion release and pH change.

In addition, the impact of metal ion doping had a role to play in terms of the cellular response observed. The Cu-doped coatings were found to be concentration dependent; in the case of moderate amounts of Cu, it was found that these would stimulate osteogenesis, whereas higher amounts would cause cytotoxicity. In the same manner, for silver, it was determined that low concentrations of silver (0.01 and 0.05 M%) could sustain cell proliferation, but in comparison to 0.1 M%, it caused cell death, almost to an extent similar to Mg itself due to increased Ag^{+} ion release (Ali *et al.* 2019).

3.9 Antimicrobial Activity

The antibacterial effectiveness of the bare and metal-doped samples of magnesium was tested using the broth dilution method for Staphylococcus aureus (Gram-positive) and Escherichia coli (Gram-negative) bacteria, and their data are shown in Fig. 3.10(a-c). The growth of bacteria was measured in time as a comparison between the treated sample and the untreated one. Generally speaking, the silver and copper doped coatings showed much better performance than bare magnesium with regard to reducing the growth of bacteria, demonstrating antibacterial effect. According to the XRD data, there were the Ag/Ag_3PO_4 phases formed in the former case and Cu-phosphate in the latter one.

Increased antibacterial action of the Ag-doped films was caused by a continuous release of Ag^{+} ions that interfere with several aspects of bacterial activities such as cell wall structure, protein production, and DNA replication. Besides, Ag^{+} leads to the oxidative stress of bacteria due to ROS formation. Of all tested compositions, the best antibacterial action and stability were provided by 0.05 M Ag; nevertheless, 0.1 M Ag showed good antibacterial behavior but was less biocompatible in cytocompatibility tests. In turn, copper-doped films were also able to demonstrate their antibacterial action via oxidative stress induced by Cu^{2+} and cell membrane disruption; yet, the effectiveness was worse at low concentrations (0.01 and 0.05 M) and improved only at higher levels (0.1 M).

In the case of AZ31 substrates, all coated samples were found to display significant enhancement in antibacterial efficiency relative to the bare alloy that displayed very little inhibition due to poor ion release. In terms of bacterial inhibition, the coatings doped with silver ions demonstrated superior performance compared to those doped with copper ions, especially at lower ion concentration ranges (0.01-0.05 M). The latter demonstrated similar inhibition at higher ion concentration (0.1 M).

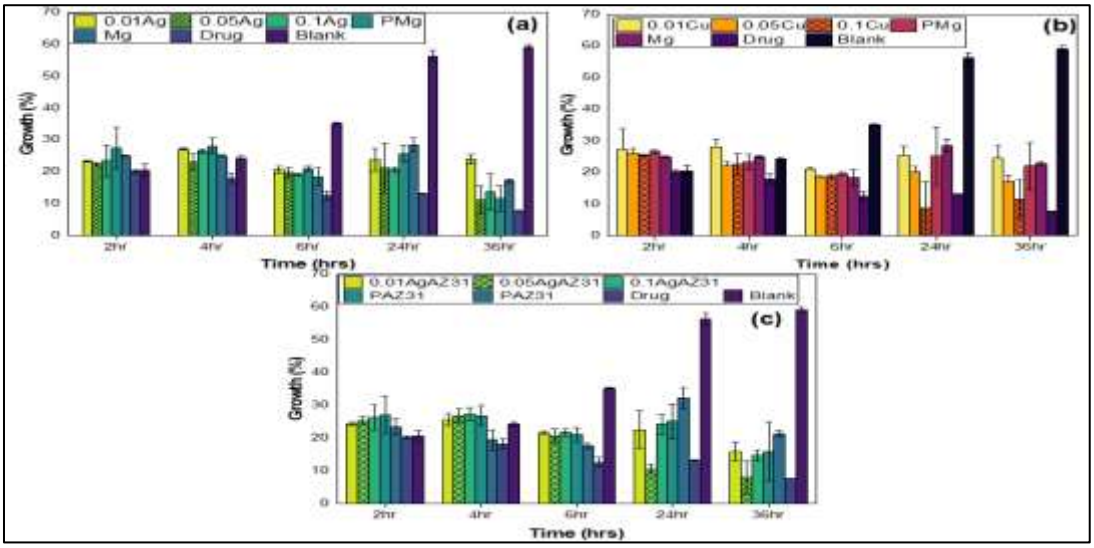

Figure 3.10 Antibacterial behavior of (a) Silver doped phosphate coated pure Mg samples on bacterial strain (b) Copper doped phosphate coated pure Mg samples on bacterial strain (c) Silver doped phosphate coated AZ31-Mg alloy on bacterial strain

4. CONCLUSION

Overall, this research has proven that phosphate coatings, synthesized using the one-step hydrothermal approach, contribute to enhanced properties of magnesium implants owing to controlled degradation and biological activity. In particular, magnesium phosphate coatings demonstrated a remarkable capacity to control corrosion kinetics and minimize hydrogen evolution. Thus, these coatings successfully ensured the maintenance of magnesium substrate integrity since they retained its mechanical characteristics, specifically around 90% of compressive strength, while meeting the criteria for mechanical performance needed for load-bearing devices. With respect to synthesis conditions, pH of the precursor solution is considered an important parameter affecting coating formation, deposition efficiency, morphology, phase distribution, and thickness. Indeed, the pH value equal to 9 with 150 °C temperature provided the preparation of dense, homogenous, and well-adherent coatings. In particular, characterization showed the presence of stable phases (brucite and $Mg_3(PO_4)_2 \cdot 12H_2O$) which contributed to improved corrosion behavior and minimized weight loss and hydrogen evolution. Biosafety tests conducted on pre-osteoblast MC3T3-E1 cells showed good cell compatibility, higher cell viability, proliferation, and adhesion rates on coated surfaces than bare magnesium surfaces and higher osteogenic gene expression levels, suggesting improved osteo-conductivity properties. In summary, the findings confirm that the one-step hydrothermal process is a straightforward and affordable method of coating production, representing an ideal way to mitigate issues related to biodegradation and hydrogen gas production by magnesium implants used in orthopedics.

Acknowledgement

The necessary funding/resources have been jointly provided by the Department of Chemistry, University of Management and Technology, Lahore, 54770 Pakistan and Ministry of Science and Technology, Government of Pakistan is acknowledged for a developmental grant (CATBM PC-1) titled "Establishment of Center for Advanced Technologies in Biomedical Materials" awarded to COMSATS University Islamabad under its knowledge economy initiative

REFERENCES

1. Al-Tamimi, A. A., P. R. A. Fernandes, C. Peach, G. Cooper, C. Diver and P. J. Bartolo (**2017**). "Metallic bone fixation implants: a novel design approach for reducing the stress shielding phenomenon." *Virtual and Physical Prototyping* 12(2): 141-151.
2. Ali, A., F. Ikram, F. Iqbal, H. Fatima, A. Mehmood, M. Y. Kolawole, A. A. Chaudhry, S. A. Siddiqi and I. U. Rehman (**2021**). "Improving the in vitro degradation, mechanical and biological properties of AZ91-3Ca Mg alloy via hydrothermal calcium phosphate coatings." *Frontiers in Materials* 8: 715104.
3. Ali, A., F. Iqbal, A. Ahmad, F. Ikram, A. Nawaz, A. A. Chaudhry, S. A. Siddiqi and I. Rehman (**2019**). "Hydrothermal deposition of high strength calcium phosphate coatings on magnesium alloy for biomedical applications." *Surface and Coatings Technology* 357: 716-727.
4. Asl, S. K. F., S. Nemeth and M. J. Tan (**2014**). "Hydrothermally deposited protective and bioactive coating for magnesium alloys for implant application." *Surface and Coatings Technology* 258: 931-937.
5. Bai, L., Y. Liu, Z. Du, Z. Weng, W. Yao, X. Zhang, X. Huang, X. Yao, R. Crawford and R. Hang (**2018**). "Differential effect of hydroxyapatite nano-particle versus nano-rod decorated titanium micro-surface on osseointegration." *Acta biomaterialia* 76: 344-358.
6. Bakin, B., T. K. Delice, U. Tiric, I. Birlik and F. A. Azem (**2016**). "Bioactivity and corrosion properties of magnesium-substituted CaP coatings produced via electrochemical deposition." *Surface and Coatings Technology* 301: 29-35.
7. Balamurugan, A., G. Balossier, S. Kannan, J. Michel, J. Faure and S. Rajeswari (**2007**). "Electrochemical and structural characterisation of zirconia reinforced hydroxyapatite bioceramic sol–gel coatings on surgical grade 316L SS for biomedical applications." *Ceramics International* 33(4): 605-614.
8. Biggs, M. J. P., R. G. Richards and M. J. Dalby (**2010**). "Nanotopographical modification: a regulator of cellular function through focal adhesions." *Nanomedicine: Nanotechnology, Biology and Medicine* 6(5): 619-633.
9. Brar, H. S., M. O. Platt, M. Sarntinoranont, P. I. Martin and M. V. Manuel (**2009**). "Magnesium as a biodegradable and bioabsorbable material for medical implants." *Jom* 61(9): 31-34.
10. Cacciotti, I., A. Bianco, M. Lombardi and L. Montanaro (**2009**). "Mg-substituted hydroxyapatite nanopowders: Synthesis, thermal stability and sintering behaviour." *Journal of the European Ceramic Society* 29(14): 2969-2978.
11. Chandra, G. and A. Pandey (**2020**). "Biodegradable bone implants in orthopedic applications: a review." *Biocybernetics and Biomedical Engineering* 40(2): 596-610.
12. D'Amado, M. P., W. Bezold, B. D. Crist and J. L. Cook (**2024**). "Biomechanical comparison of traditional plaster cast and 3D-printed orthosis for external coaptation of distal radius fractures." *Annals of 3D Printed Medicine* 14: 100146.
13. Farjam, P., E. Hekman, J. Rouwkema and G. Verkerke (**2022**). "Bone fixation techniques for managing joint disorders and injuries: A review study." *journal of the mechanical behavior of biomedical materials* 126: 104982.

14. Gefen, A. (**2002**). "Computational simulations of stress shielding and bone resorption around existing and computer-designed orthopaedic screws." *Medical and Biological Engineering and Computing* 40(3): 311-322.
15. Gray-Munro, J. E., C. Seguin and M. Strong (**2009**). "Influence of surface modification on the in vitro corrosion rate of magnesium alloy AZ31." *Journal of Biomedical Materials Research Part A: An Official Journal of The Society for Biomaterials, The Japanese Society for Biomaterials, and The Australian Society for Biomaterials and the Korean Society for Biomaterials* 91(1): 221-230.
16. Gueorguiev, B., F. T. Moriarty, M. Stoddart, Y. P. Acklin, R. G. Richards and M. Whitehouse (2017). Principles of fractures. Apley & Solomon's System of Orthopaedics and Trauma, CRC Press**:** 711-754.
17. Hiromoto, S. and A. Yamamoto (**2009**). "High corrosion resistance of magnesium coated with hydroxyapatite directly synthesized in an aqueous solution." *Electrochimica Acta* 54(27): 7085-7093.
18. Hiromoto, S., A. Yamamoto, N. Maruyama, H. Somekawa and T. Mukai (**2008**). "Influence of pH and flow on the polarisation behaviour of pure magnesium in borate buffer solutions." *Corrosion Science* 50(12): 3561-3568.
19. Hornberger, H., S. Virtanen and A. R. Boccaccini (**2012**). "Biomedical coatings on magnesium alloys–a review." *Acta biomaterialia* 8(7): 2442-2455.
20. Jin, Y., J. Li, H. Fan, J. Du and Y. He (**2025**). "Biomechanics and Mechanobiology of Additively Manufactured Porous Load-Bearing Bone Implants." *Small* 21(20): 2409955.
21. Kokubo, T. and H. Takadama (**2007**). "Simulated body fluid (SBF) as a standard tool to test the bioactivity of implants." *Handbook of biomineralization: biological aspects and structure formation*: 97-109.
22. Lian, J. B. and G. S. Stein (**1992**). "Concepts of osteoblast growth and differentiation: basis for modulation of bone cell development and tissue formation." *Critical Reviews in Oral Biology & Medicine* 3(3): 269-305.
23. Liu, C., X. Fu, H. Pan, P. Wan, L. Wang, L. Tan, K. Wang, Y. Zhao, K. Yang and P. K. Chu (**2016**). "Biodegradable Mg-Cu alloys with enhanced osteogenesis, angiogenesis, and long-lasting antibacterial effects." *Scientific Reports* 6(1): 27374.
24. Liu, W., T. Wang, C. Yang, B. Darvell, J. Wu, K. Lin, J. Chang, H. Pan and W. Lu (**2016**). "Alkaline biodegradable implants for osteoporotic bone defects—importance of microenvironment pH." *Osteoporosis International* 27(1): 93-104.
25. Matli, P. R., A. V. Krishnan, V. Manakari, G. Parande, B. Chua, S. Wong, C. Lim and M. Gupta (**2020**). "A new method to lightweight and improve strength to weight ratio of magnesium by creating a controlled defect." *Journal of Materials Research and Technology* 9(3): 3664-3675.
26. Misir, A. (**2025**). "Current developments in orthopaedic implant technology." *Journal of Orthopaedic Surgery and Research* 20(1): 927.
27. Muralidharan, S., M. Gore and S. Katkuri (**2023**). "Cancer care and economic burden—A narrative review." *Journal of Family Medicine and Primary Care* 12(12): 3042-3047.
28. Niyou, W. (2021). An investigation on low-elastic-modulus metallic orthopedic implants, National University of Singapore (Singapore).
29. Noviana, D., D. Paramitha, M. F. Ulum and H. Hermawan (**2016**). "The effect of hydrogen gas evolution of magnesium implant on the postimplantation mortality of rats." *Journal of Orthopaedic Translation* 5: 9-15.
30. Nuss, K. M. and B. von Rechenberg (**2008**). "Biocompatibility issues with modern implants in bone-a review for clinical orthopedics." *The open orthopaedics journal* 2: 66.
31. Paiva, J. C., L. Oliveira, M. F. Vaz and S. Costa-de-Oliveira (**2022**). "Biodegradable bone implants as a new hope to reduce device-associated infections—a systematic review." *Bioengineering* 9(8): 409.
32. Prakasam, M., J. Locs, K. Salma-Ancane, D. Loca, A. Largeteau and L. Berzina-Cimdina (**2017**). "Biodegradable materials and metallic implants—a review." *Journal of functional biomaterials* 8(4): 44.
33. Prawin Babu, L. and R. Radha (**2025**). "Advancements in magnesium-based alloys for orthopedic implants: balancing corrosion, mechanical properties, and biological effects (part 1)–a review." *Canadian Metallurgical Quarterly* 64(4): 2039-2064.
34. Radha, R. and D. Sreekanth (**2017**). "Insight of magnesium alloys and composites for orthopedic implant applications–a review." *Journal of magnesium and alloys* 5(3): 286-312.
35. Rahim, M. I., A. Tavares, F. Evertz, M. Kieke, J. M. Seitz, R. Eifler, A. Weizbauer, E. Willbold, H. Jürgen Maier and B. Glasmacher (**2017**). "Phosphate conversion coating reduces the degradation rate and suppresses side effects of metallic magnesium implants in an animal model." *Journal of Biomedical Materials Research Part B: Applied Biomaterials* 105(6): 1622-1635.
36. Schatzker, J. (2005). Principles of internal fixation. The rationale of operative fracture care, Springer**:** 3-31.
37. Schlickewei, C. W., H. Kleinertz, D. M. Thiesen, K. Mader, M. Priemel, K.-H. Frosch and J. Keller (**2019**). "Current and future concepts for the treatment of impaired fracture healing." *International journal of molecular sciences* 20(22): 5805.
38. Shadanbaz, S. and G. J. Dias (**2012**). "Calcium phosphate coatings on magnesium alloys for biomedical applications: a review." *Acta biomaterialia* 8(1): 20-30.

39. Sharma, S. K., K. K. Saxena, V. Malik, K. A. Mohammed, C. Prakash, D. Buddhi and S. Dixit (**2022**). "Significance of alloying elements on the mechanical characteristics of Mg-based materials for biomedical applications." *Crystals* 12(8): 1138.
40. Song, G. (**2005**). "Recent progress in corrosion and protection of magnesium alloys." *Advanced engineering materials* 7(7): 563-586.
41. Song, G. (**2007**). "Control of biodegradation of biocompatable magnesium alloys." *Corrosion science* 49(4): 1696-1701.
42. Song, G. and S. Song (**2007**). "A possible biodegradable magnesium implant material." *Advanced engineering materials* 9(4): 298-302.
43. Staiger, M. P., A. M. Pietak, J. Huadmai and G. Dias (**2006**). "Magnesium and its alloys as orthopedic biomaterials: a review." *Biomaterials* 27(9): 1728-1734.
44. Stiffler, K. S. (**2004**). "Internal fracture fixation." *Clinical Techniques in Small Animal Practice* 19(3): 105-113.
45. Sui, J.-L., M.-S. Li, Y.-P. Lü, L.-W. Yin and Y.-J. Song (**2004**). "Plasma-sprayed hydroxyapatite coatings on carbon/carbon composites." *Surface and Coatings Technology* 176(2): 188-192.
46. Sun, J., C. Chen, B. Zhang, C. Yao and Y. Zhang (**2025**). "Advances in 3D-printed scaffold technologies for bone defect repair: materials, biomechanics, and clinical prospects." *Biomedical engineering online* 24(1): 51.
47. Tabrizian, P., S. Davis and B. Su (**2024**). "From bone to nacre–development of biomimetic materials for bone implants: a review." *Biomaterials Science* 12(22): 5680-5703.
48. Tang, H., T. Xin and F. Wang (**2013**). "Calcium phosphate/titania sol-gel coatings on AZ31 magnesium alloy for biomedical applications." *International Journal of Electrochemical Science* 8(6): 8115-8125.
49. Uppal, G., A. Thakur, A. Chauhan and S. Bala (**2021**). "Magnesium based implants for functional bone tissue regeneration–A."
50. Vos, D. and M. Verhofstad (**2013**). "Indications for implant removal after fracture healing: a review of the literature." *European Journal of Trauma and Emergency Surgery* 39(4): 327-337.
51. Witte, F., V. Kaese, H. Haferkamp, E. Switzer, A. Meyer-Lindenberg, C. J. Wirth and H. Windhagen (**2005**). "In vivo corrosion of four magnesium alloys and the associated bone response." *Biomaterials* 26(17): 3557-3563.
52. Xu, L., X. Liu, K. Sun, R. Fu and G. Wang (**2022**). "Corrosion behavior in magnesium-based alloys for biomedical applications." *Materials* 15(7): 2613.
53. Yadav, S., J. Yadav, S. Kumar and P. Singh (2024). Metabolism of macro-elements (calcium, magnesium, sodium, potassium, chloride and phosphorus) and associated disorders. Clinical applications of biomolecules in disease diagnosis: A comprehensive guide to biochemistry and metabolism, Springer**:** 177-203.